Desalination and Water Treatment
www.deswater.com

doi: 10.1080/19443994.2015.1088805

57 (2016) 18354–18365
August

Taylor & Francis
Taylor & Francis Group

The preparation of a cross-linked cerium (III)-loaded alginate bead adsorbent for the removal of phosphate from wastewater

Heng Yang[a,b], Qi Zhou[a,b], Wenjun Luo[a], Chunjie Yan[a,b,*], Chunyu Zhou[a,b]

[a]*Faculty of Material and Chemistry, China University of Geosciences, Wuhan 430074, P.R. China, emails: yh061053@126.com (H. Yang), roundzking@163.com (Q. Zhou), heartnohome@126.com (W. Luo), Tel./Fax: +86 27 67885098; emails: chjyan2005@126.com (C. Yan), zhouchunyu1988@126.com (C. Zhou)*

[b]*Engineering Research Center of Nano-Geomaterials of Education Ministry, China University of Geosciences, Lu Mo Road 388, Wuhan 430074, P.R. China*

Received 29 January 2015; Accepted 24 August 2015

ABSTRACT

The aim of this study was to prepare a cross-linked cerium(III)-loaded alginate bead (denoted as SA-Ca-Ce) and to apply it to remove phosphate from aqueous solution. The adsorption behaviors were investigated by the batch experiments at various experimental parameters including contact time, initial phosphate concentration, solution pH, temperature, and coexisting anions. The results showed that the Langmuir model is more suitable than the Freundlich model for well elucidation of the experimental data, and the maximum adsorption capacity is calculated to be 41.39 mg/g at 318 K. The adsorption of phosphate, which followed pseudo-second-order kinetics, is a chemisorption process. The phosphate adsorption had a slight decrease with the increasing of pH. The coexistence of other anions in solutions has an adverse effect on phosphate adsorption with the extent following the order: $HCO_3^- > SO_4^{2-} > Cl^-$. The phosphate adsorption mechanism was also investigated by scanning electron microscopy, Fourier transform infrareds spectroscopy. The electrostatic interactions and Lewis acid ligand were manifested to be two main mechanisms for phosphate adsorption onto SA-Ca-Ce. All the results indicated that the SA-Ca-Ce has a considerable potential for the phosphate removal from contaminated waters.

Keywords: Phosphate; Adsorption; Cerium; Alginate bead; Mechanism

1. Introduction

Eutrophication, which leads to the abundance of aquatic plants, growth of algae, and depletion of dissolved oxygen, has become a global environmental problem [1]. Recent studies have confirmed that the amounts of soluble phosphate in water body from households, agriculture, and industries are the main cause for eutrophication; thus controlling the discharge of wastewater containing phosphate can be an effective way to control eutrophication [2,3]. Various methods have been applied to remove phosphate from water and wastewater, including chemical precipitation, biological processes [4], ion exchange [5,6], and adsorption [7,8]. Among them, adsorption is considered to be one of the most attractive approaches with the advantage of high removal efficiency, simple operation, and economy in application, wherein development of high-quality phosphate adsorbents is

*Corresponding author.

the key. In the last decade, numerous phosphate adsorbents have been studied including dolomite [9], polymeric ligand exchanger [10], aluminum and aluminum (hydroxide) [11,12], zeolites [13], blast furnace slag [14], red mud [15,16], mesoporous silicates [11,17], iron oxides [18], fly ash [19], and so on. However, these adsorbents often suffer from the shortage of low adsorption capacities, separation inconvenience, and the complicated preparation process [20,21]. Therefore, efforts still need to be made to investigate the new and promising adsorbents.

The rare earth adsorbents have been attracting more and more attention for their high affinity to phosphate, high adsorption capacity, little pollution, easy operation, and other merits [22]. But the cost is very high and the collection is difficult by the direct use of rare earth compounds to deal with the phosphate wastewater. In recent years, considerable amount of work has been done on developing composite adsorbents based on rare earth elements for the removal of phosphate. For example, lanthanum-doped vesuvianite [23], cerium-impregnated fibrous protein [24], lanthanum/lanthanum hydroxide-doped activated carbon fiber [20,25], expanded graphite loaded with lanthanum oxide [26], and mixed lanthanum/aluminum-pillared montmorillonite [27]. However, the treatment of waste adsorbent has always been a persistent problem.

On the other hand, there is a growing interest in the biopolymer in the form of beads or granules with optimum size, rigidity, and porosity characteristics [28] for the wastewater treatment. Alginate, a biodegradable, biocompatible, and low-cost biomaterial, is a linear polyuronate obtained from marine algae that contains variable amounts of d-manuronic acid and l-guluronic acid, which can be cross-linked using calcium ion. Cross-linked alginate material exhibits strong mechanical strength and have been applied to the removal of hazardous ions [29].

The main objective of this study was to prepare a novel adsorbent by impregnating cross-linked alginate with Ce^{3+} (maximum abundance in rare earth elements) and analyze the performance of the adsorbent for removing phosphate from water. The composite adsorbent was processed to a granular shape via drop-sphere-forming method, which has the adsorption capacity of 41.39 mg/g at the optimal conditions. Alginate bead can maintain stable network structure at the acidic region. What is more, it is worth noting that micro-rare earth ions have beneficial effects on plant growth [30], so the adsorbent after P saturated adsorption can be recycled and used as cheap and degradable phosphate/Ce^{3+} compound fertilizer without further treatment. The objectives of this investigation are as follows: (i) to prepare a novel cerium(III)-loaded hyper-cross-linked alginate (SA-Ca-Ce) bead adsorbent; (ii) to systematically study the adsorption characteristics SA-Ca-Ce bead in batch experiment as a function of pH, coexisting anions, contact time, ion concentration, and temperature; (iii) to reveal the mechanisms of phosphate adsorption onto SA-Ca-Ce bead. Results of this research demonstrate that SA-Ca-Ce bead has excellent properties in the phosphate removal.

2. Experimental procedures

2.1. Materials

All the chemicals including sodium alginate (SA), anhydrous calcium chloride, cerium nitrate, sodium sulfate, sodium chloride, and sodium fluoride were reagent grade from Sinopharm Chemical Reagent Co., Ltd, (China), and used without further purification.

2.2. Preparation of SA-Ca-Ce beads

The SA solution was obtained by dissolving SA (2 g) into deionized water (100 ml) slowly through magnetic stirring. Then, the alginate colloidal solution was left for 30 min to let the bubbles disappear.

As shown in Fig. 1, the preparation method of SA-Ca-Ce bead was as follows: After being defoamed, SA solution was dripped into the 0.05 mol/L $CaCl_2$ solution with 50 mL medical syringe without the needle. An optimal drop height to obtain spherical beads was 6.0 cm [31]. The products formed in the $CaCl_2$ solution were the cross-linked SA-Ca beads. These beads were left in the $CaCl_2$ solution for 12 h, so that the gelation process had enough time to be carried out in the whole bead. After the curing period, the beads were washed three times with distilled water to remove the unbound Ca^{2+}. SA-Ca-Ce beads were prepared by soaking SA-Ca beads in the cerium nitrate solution (0.02 mol/L) for another 12 h. To avoid the collapse of the internal structure, the wet beads (SA-Ca-Ce) were stored in 0.01 mol/L HCl solution and used without drying [32].

2.3. Characterization of the SA-Ca-Ce bead

Surface morphologies of SA-Ca-Ce beads and SA-Ca-Ce-P (SA-Ca-Ce after phosphate adsorption) beads were observed by a scanning electron microscopy (SEM) using a SU8010 instrument (Hitachi Co. Ltd, Japan). Fourier transform infrared (FT-IR) measurements (mid-infrared absorption spectrum) were performed on a VERTEX 70 instrument (Bruker Co.

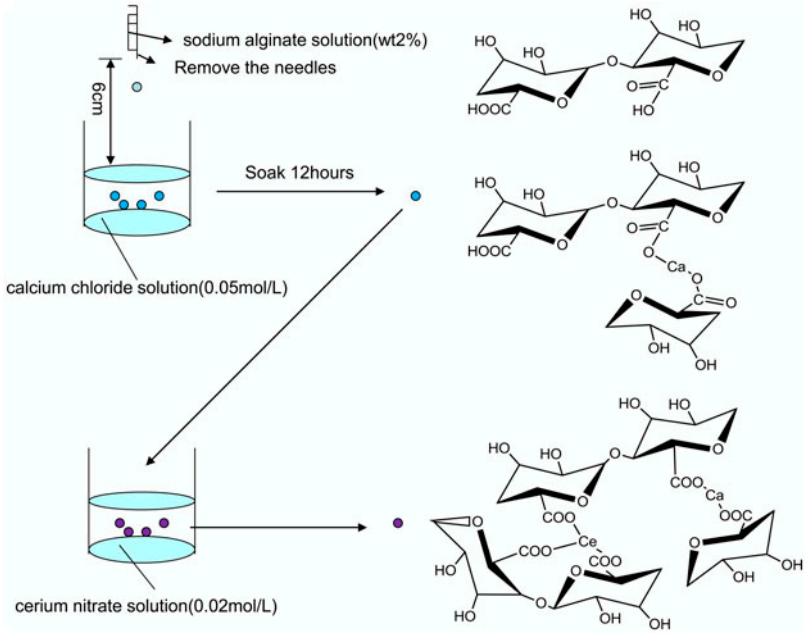

Fig. 1. The preparation process diagram of SA-Ca-Ce beads.

Ltd, GER). Information about the surface charge of this material was obtained by zeta potential measurements using a nano ZS90 instrument (Malvern Co. Ltd, UK).

2.4. Phosphate adsorption experiments with SA-Ca-Ce beads

The stock phosphate solution (100 mg/L) was obtained by dissolving 0.8788 g of dihydrogen phosphate (KH_2PO_4) in a 2-L volumetric flask using deionized water. All solutions for the phosphate removal experiments were prepared by an appropriate dilution from the stock solution. Adsorption processes for the phosphate removal experiments were conducted as follows: Adsorption was carried out by adding 0.02 g (dry weight) of the adsorbent into 20 mL vial with 10 mL of P solution. The vials were placed in a thermostatic shaker bath for several predetermined temperatures and shaken at 120 rpm. At the end of adsorption process, the solutions were filtered and tested for P concentration.

To investigate the influence of pH on phosphate adsorption, initial pH of P solution with the concentration of 100 mg/L was adjusted from 2.0 to 6.0 using 1 mol/L NaOH and HCl solution. Three sets of adsorption kinetic experiments with different initial concentrations (30, 60, and 100 mg/L, respectively) were conducted by varying the contact time from 20 to 540 min at pH 2.0 and under 298 K. As for the equilibrium experiments, the similar aforementioned experimental procedures over a range of initial phosphate concentrations from 10 to 100 mg/L were performed at three temperatures (298, 308, and 318 K, respectively). In addition, the effect of coexisting anions on the phosphate adsorption process was also explored by adding various competing anions of SO_4^{2-}, Cl^-, and HCO_3^- (0.5 and 5 mol/L).

2.5. Analytical methods

The concentrations of the phosphate solutions were determined by the ascorbic acid method. The absorbance of the solutions was analyzed by UV-1800PC spectrophotometer (Shanghai Mapada Instruments Co. Ltd, China). The pH of the solution was determined by Sartorius PB220 pH meter (Sartorius, Ger).

The adsorption capability (Q_e, mg/g) of phosphate in SA-Ca-Ce bead was calculated by the following equation:

$$Q_e = \frac{(C_0 - C_e)V}{m} \quad (1)$$

where C_0 and C_e (mg/L) are the initial and equilibrium liquid phase phosphate concentrations, respectively; V (L) is the volume of the solution, and m (g) is the mass of the adsorbent.

2.6. Stability of the SA-Ca-Ce beads

To determine the loss rate of Ce^{3+} and Ca^{2+} after adsorption process, the content of Ce^{3+} and Ca^{2+} in the SA-Ce-Ca was investigated before and after the addition of adsorbent in the P solution at 100 mg/L with the dosage of 2 g/L. The residual solution was collected after filtration at the end of the adsorption process. The adsorbent was burned at 873K in an oven, and the residue was dissolved with 1 mol/L of sulfuric acid solution. Then, the concentration of Ce^{3+} and Ca^{2+} in these solutions was analyzed by DGS-III single channel scanning spectrometer instrument (Shanghai Tailun Co. Ltd, China).

3. Results and discussion

3.1. Characterization

The SEMs of the cross section of SA-Ca-Ce at before and after the phosphate adsorption (denoted as SA-Ca-Ce-P) are shown in Fig. 2. As is shown, apparent differences are found between the two images that SA-Ca-Ce exhibits a smooth cross section, while the cross section of SA-Ca-Ce-P changed to a morphology as cellular network after the phosphate adsorption, which indicates that the bonds of cross-linking network (SA-Ca-Ce) were broken and got new bonds with the PO_4^{3-} on the Ce^{3+}/Ca^{2+} sites for a certain degree in the process of adsorption. The EDS analysis for element of adsorbent is shown in Fig. 2(c) and (d). The results show that Ce^{3+} should be the main sites to form the cross-linked structure of alginate bead than Ca^{2+} ion owing to the relatively high content, which make excellent mechanical property of the beads. Furthermore, the element of phosphate is found in Fig. 2(d), illustrating that phosphate had been adsorbed into SA-Ca-Ce bead.

FT-IR spectra of SA-Ca-Ce bead and SA-Ca-Ce-P bead are represented in Fig. 3, and Table 1 shows the possible assignments for the FT-IR bands of the alginate salts. From Fig. 3(a), the bands corresponding to the presence of SA-Ca-Ce bead, namely at 3,315 cm^{-1} (νOH), 1,587 and 1,410 cm^{-1} (νCOO^-), and 820 cm^{-1} identified in the literature as the combination of three

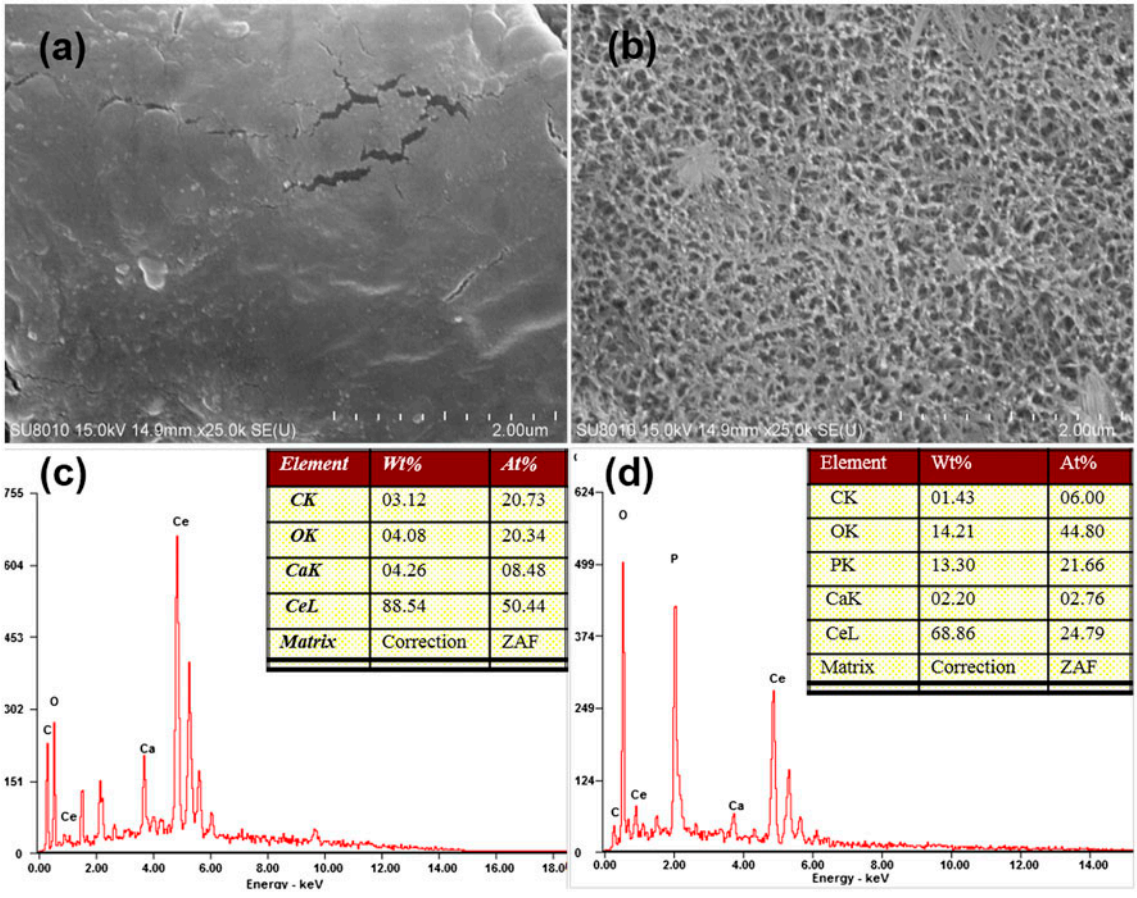

Fig. 2. SEM of (a) SA-Ca-Ce bead and (b) SA-Ca-Ce-P bead, EDS analysis of (c) SA-Ca-Ce bead and (d) SA Ca-Ce-P bead.

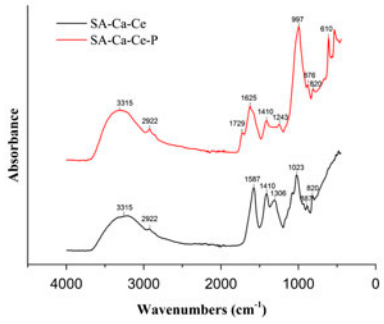

Fig. 3. FT-IR spectra of SA-Ca-Ce and SA-Ca-Ce-P.

material (SA-Ca-Ce) is at about pH 3, indicating that when pH > 3, material surface charge is negative, while material surface has positive charge below pH 3.0.

3.2. Adsorption properties

3.2.1. Effect of pH on adsorption of phosphate

The effect of initial pH on the phosphate removal was shown in Fig. 5, where the pH range of 2.0–6.0 was considered only, because that alginate beads become unstable due to swelling under the condition of alkaline. It is shown that the phosphate adsorption capacity of the SA-Ca-Ce bead had a slow decline with the increasing solution pH. It is well known that PO_4^{3-} as a kind of anion is more likely to be attracted by positively charged surface. As previously stated, material surface is positively charged when pH < 3, so that pH 2 is regarded as the optimum pH condition. Moreover, it is worth noting that there is still a certain adsorption capacity even at pH below 3.2, which

Table 1
Peak assignment of absorption bands of SA-Ca-Ce and SA-Ca-Ce-P spectra obtained by FT-IR

Na/Ca-alginte bands (cm^{-1})	Peak assignment	Na/Ca-alginte bands (cm^{-1})	Peak assignment
3,315	ν(OH)hydrogen bonded	1,306/1,243	$\nu(COO^-)$
2,922	ν(CH)	1,023/997	τ(CO), δ(CCO), δ(CC)
1,729	ν(PO)	887/876	ν(CO), δ(CCH)
1,625/1,587	$\nu(COO^-)$	820	τ(CO), δ(CCO), δ(CCH)
1,410	$\nu(COO^-)$	610	$\beta(PO_4^{3-})$

possible vibrational modes (τCO + δCCO + δCCH), can be observed [33]. Compared with SA-Ca-Ce bead, some new peaks were appeared in SA-Ca-Ce-P, including the P-O stretching vibration at 1,729 cm^{-1}, PO_4^{3-} in-plane flexural vibration at 610 cm^{-1} and a signal stretch at 900–1,200 cm^{-1} corresponding to the νPO_4^{3-} region [34], which further confirmed the successful adsorption of phosphate.

To obtain information about the surface charge of this material, zeta potential measurements were carried out at various pH values (pH 1.0–6.0). As shown in Fig. 4, it can be found that the zero potential of the

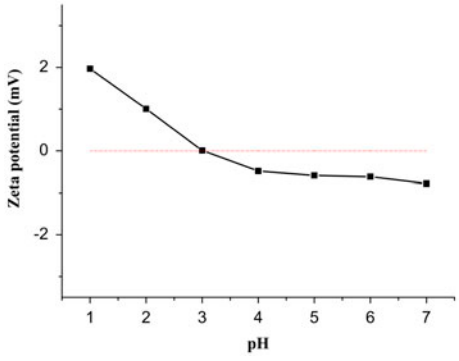

Fig. 4. Zeta-potential of SA-Ca-Ce beads.

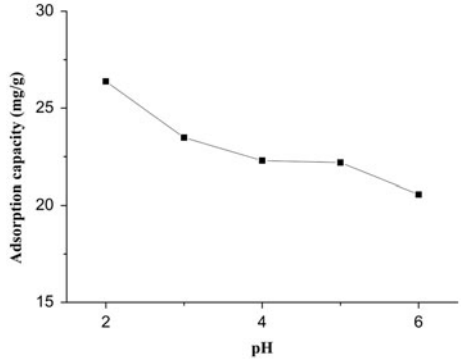

Fig. 5. Adsorption capacity of initial pH on phosphate adsorption in beads. Initial phosphate concentration of 100 mg/L, adsorbent dosage 2.0 g/L and temperature = 298 K.

should be due to the Lewis acid ligand interactions existed between the adsorption sites and phosphate.

3.2.2. Adsorption kinetic studies

Kinetic studies were carried out to determine the phosphate removal from solution by SA-Ca-Ce beads. Fig. 6(a) illustrates the change of adsorption amount as a function of initial phosphate concentration (30, 60, 100 mg/L) and contact time. All three curves exhibit the same trend. The maximum phosphate adsorption amount is found to be 12.0, 18.9, and 27.25 mg/g for different initial concentrations at room temperature, respectively. The adsorption process was divided into two stages: When contact time is less than 4 h, the adsorption capacity increased rapidly and then reached equilibrium.

Kinetic data were then represented by the pseudo-first-order and second-order models as Eqs. (2) and (3):

$$\log(q_e - q_t) = \log q_e - \frac{k_1 t}{2.303} \quad (2)$$

$$\frac{t}{q_t} = \frac{1}{k_2 q_e^2} + \frac{t}{q_e} \quad (3)$$

where q_e (mg/g) and q_t (mg/g) are the amount of phosphate adsorbed on sorbent at equilibrium and at time t (min), respectively; k_1 is the adsorption rate constant of pseudo-first-order adsorption, k_2 (g/mg min) is the equilibrium rate constant of pseudo-second-order adsorption [35,36]. The pseudo-first-order and the pseudo-second-order plots for the adsorption of the phosphate on the adsorbent are shown in Fig. 6(b) and (c), respectively.

The values of kinetic parameters as well as corresponding correlation coefficients are shown in Table 2. According to a high value of the correlation coefficient ($R^2 > 0.999$), it can be concluded that pseudo-second-order adsorption model is more suitable for the description of the adsorption kinetics of phosphate on SA-Ca-Ce bead, indicating that the adsorption of phosphate is a chemisorption process [37].

Intraparticle diffusion mechanism is one of the most limiting factors which controlled adsorption kinetics [38,39]. In order to determine the actual rate-controlling step involved in the phosphate adsorption process, the well-known Weber–Morris equation was applied as Eq. (4) [39]:

$$q_t = k_i t^{0.5} + b \quad (4)$$

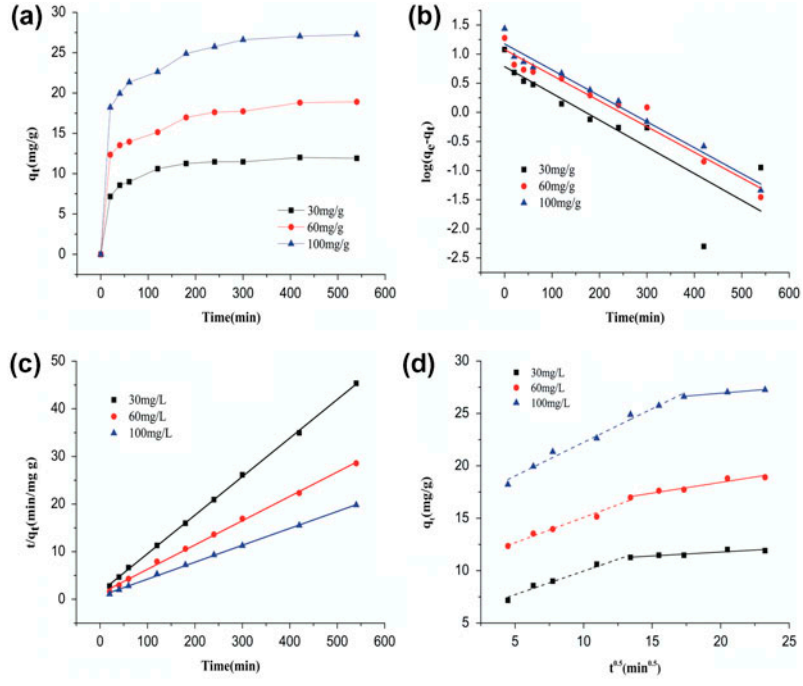

Fig. 6. (a) effect of contact time and initial concentration, adsorbent dosage 2.0 g/L, pH 2.0 and temperature = 298 K, (b) pseudo-first-order plots, (c) pseudo-second-order plots and (d) intraparticle diffusion model plots for adsorption of phosphate on the adsorbent.

Table 2
Comparison of the first- and second-order adsorption rate constants and experimental values for different initial phosphorus concentrations

	First-order kinetics			Second-order kinetics		
Initial concentration C_0 (mg/L)	k_1 (min^{-1})	$q_{e(cal)}$ (mg/g)	R^2	k_2 (g/(mg min))	$q_{e(cal)}$ (mg/g)	R^2
30	0.01	6.09	0.717	0.004	12.36	0.999
60	0.01	11.92	0.952	0.002	19.58	0.999
100	0.01	14.95	0.972	0.002	28.15	0.999

where q_t is the adsorption capacity (mg/g) at time t, t is the contact time (min), b (mg/g) is the intercept, and k_i is the intraparticle diffusion rate constant (mg/g $min^{0.5}$), which can be calculated from the slope of the linear plots of q_t vs. $t^{0.5}$.

For using solid adsorbent, the adsorption process may be controlled by one or more steps, such as bulk diffusion, boundary layer (film) or external diffusion, pore diffusion, surface diffusion, and adsorption onto the pore surface. Generally, the adsorption rate is controlled by outer or inner diffusion, or both. Multi-linear plots are observed in Fig. 6(d), indicating that two steps took place during phosphate adsorption onto SA-Ca-Ce beads. At early stage of the adsorption, phosphate in aqueous solution was transported onto the surface of SA-Ca-Ce beads (film diffusion), and then, phosphate was transported and adsorbed on the interior surface of the SA-Ca-Ce beads. That means outer diffusion and inner has a combined influence on adsorption rate. The intercept and slope values of two straight lines as well as R^2 values are listed in Table 3. As shown in Table 3, the intercept values b_2 are 10.28, 14.32, and 24.74 (mg/g), corresponding to various initial phosphate concentrations (30, 60, and 100 mg/L, respectively). This indicates that the boundary layer thickness increased with increasing initial phosphate concentration from 30 to 100 mg/L.

3.2.3. Adsorption isotherm models

Phosphate adsorption isotherm was obtained by varying the initial concentration of phosphate (10–200 mg/L) at three different temperatures. Absorption isotherm is described in Fig. 7(a), where q_e increases sharply at low equilibrium concentrations, and becomes flat at higher values of C_e. Fig. 7(a) also reveals that the adsorption capacity of SA-Ca-Ce bead increased with temperature. Langmuir and Freundlich equations were applied to describe the adsorption isotherm data by linear regression forms:

$$\frac{C_e}{q_e} = \frac{1}{Q_0 K_L} + \left(\frac{1}{Q_0}\right) C_e \tag{5}$$

$$\log q_e = \log K_F + \frac{1}{n} \log C_e \tag{6}$$

where C_e (mg/L) is the concentration of the phosphate solution at equilibrium, q_e (mg/g) is the amount of the phosphate absorbed by per unit of the adsorbent, and Q_0 (mg/g) and K_L (L/mg) are Langmuir constants related to the maximum monolayer adsorption and the energy of the adsorption for an adsorbent material, respectively, which are obtained by the fitting curve of C_e/q_e vs. C_e (as shown in Fig. 7(b)). K_F (mg/g) and n

Table 3
Intraparticle diffusion model for phosphate adsorption for different initial concentrations

	Whole process			First stage			Second stage		
Initial concentration C_0 (mg/L)	b (mg/g)	k_i (mg/(g $min^{0.5}$))	R^2	b_1 (mg/g)	$k_{i,1}$ (mg/(g $min^{0.5}$))	R^2	b_2 (mg/g)	$k_{i,2}$ (mg/(g $min^{0.5}$))	R^2
30	7.14	0.24	0.824	5.47	0.45	0.97	10.28	0.07	0.937
60	11.26	0.37	0.946	10.26	0.48	0.97	14.32	0.21	0.925
100	17.20	0.50	0.917	15.83	0.64	0.98	24.74	0.11	0.956

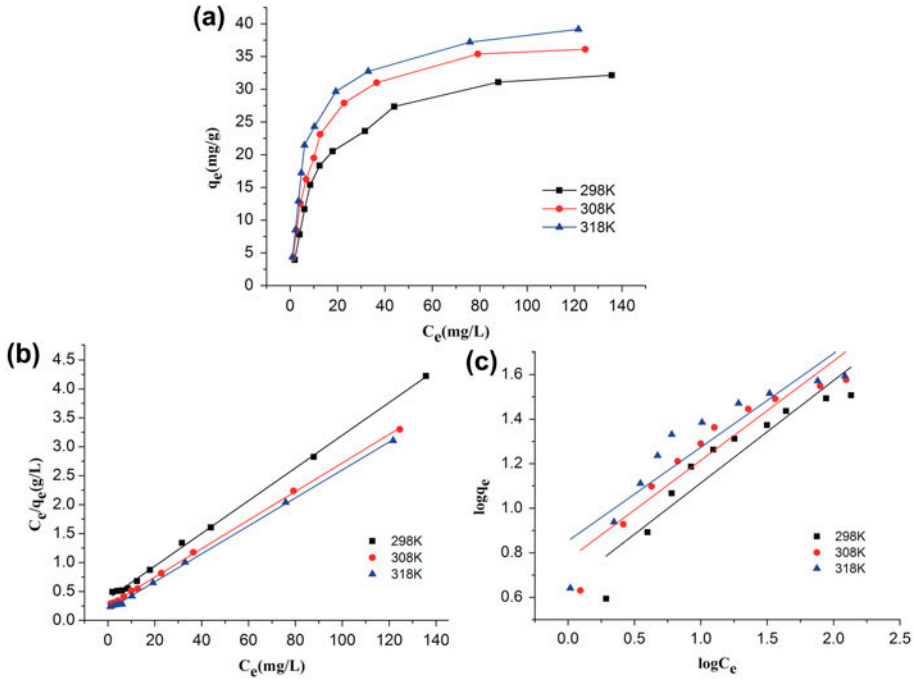

Fig. 7. (a) Isotherms of phosphate on SA-Ca-Ce bead, (b) linear Langmuir adsorption isotherms and (c) Freundlich adsorption isotherms.

are the constants of a Freundlich isotherm characterizing the adsorption capacity and intensity of adsorption, respectively, which are obtained by fitting the curve of log q_e vs. log C_e, as shown in Fig. 7(c).

The estimated adsorption constants with correlation coefficient obtained from the isotherm are listed in Table 4. In terms of the correlation coefficients R^2 values, the experimental data could be well fitted to the Langmuir isotherm model rather than the Freundlich model, indicating that the adsorption process occurred on the surface of SA-Ca-Ce should be monolayer adsorption. The maximum adsorption capacity calculated by Langmuir model is 41.39 mg/g. A comparative study of our prepared SA-Ca-Ce to several reported rare earth compounds is performed in Table 5. It is evident that the SA-Ca-Ce should have high affinity for phosphate.

Table 5
Maximum adsorption capacities for the phosphate onto various rare earth compounds

Adsorbent	Adsorption capacity (mg/g)	Refs.
EG-LaO	10.03	[26]
La-Ves	6.7	[23]
ACF-LaFe	29.44	[20]
ACF-LaOH	15.3	[25]
LaAl-PILC	8.9	[27]
SA-Ca-Ce	41.39	This work

3.2.4. Thermodynamic analysis

Valuable information of the adsorption process can be obtained through the thermodynamic parameters

Table 4
Comparison of Langmuir and Freundlich adsorption isotherm models

	Langmuir			Freundlich		
Temperature (K)	Q_0 (mg/g)	K_L (L/mg)	R^2	n	K_F (mg/g)	R^2
298	35.37	0.08	0.988	2.17	4.49	0.865
308	40.50	0.09	0.999	2.24	5.87	0.886
318	41.39	0.13	0.992	2.36	7.12	0.831

Table 6
Thermodynamic parameters for the adsorption

T (K)	Initial concentration C_0 (mg/L)	Thermodynamic parameters			
		K_c	ΔG° (kJ/mol)	ΔH° (kJ/mol)	ΔS° (kJ/(molK))
318	10	6.94	−5.12	25.21	0.096
308	10	5.85	−4.52		
298	10	3.67	−3.22		

including change in the Gibbs free energy (ΔG°), enthalpy (ΔH°), and entropy (ΔS°). ΔG° is the fundamental criterion of spontaneity. Adsorption process can be considered as an endothermic process if ΔH° is positive, and ΔS° reflects the degree of disorder and random during adsorption process.

As well known, ΔG° is related to the equilibrium constant by the classical van't Hoff equation [40]:

$$\Delta G^\circ = -RT \ln K_c \tag{7}$$

where R is the universal gas constant (8.314 J/mol K), and T is absolute temperature in Kelvin. The apparent equilibrium constant K_c of the adsorption is defined as [41,42]:

$$K_c = \frac{C_{ad,e}}{C_e} \tag{8}$$

where $C_{ad,e}$ is the concentration of phosphate on the adsorbent at equilibrium (mg/L), and C_e is the equilibrium concentration of phosphate (mg/L) in solution. The value of K_c can be obtained in the lowest experimental phosphate concentration.

The relationship of ΔH° and ΔS° can be calculated by the following equation:

$$\ln K_c = -\frac{\Delta H^\circ}{RT} + \frac{\Delta S^\circ}{R} \tag{9}$$

where ΔH° and ΔS° are calculated from the slope and intercept of the linear plot of $\ln K_c$ vs. $1/T$.

Adsorption experiments were conducted at 298, 308, and 318 K, respectively. Thermodynamic parameters obtained are listed in Table 6. From Table 6, the negative values of ΔG° confirm the spontaneous nature of the adsorption. In addition, positive values of ΔH° suggest that the interaction of phosphate adsorbed by SA-Ca-Ce is endothermic, which is supported by the increasing adsorption capacity of phosphate with the rising of temperature.

3.2.5. Competing effect of co-existing anions

The effect of coexisting anions (SO_4^{2-}, Cl^-, and HCO_3^-) on phosphate adsorption was examined. As shown in Fig. 8, the three competitive anions have different adverse effects in the phosphate removal. The inhibition in phosphate adsorption follows the order: $HCO_3^- > SO_4^{2-} > Cl^-$. Fig. 8 also reveals that there is a decrease in the phosphate removal when the concentration of the competitive ions increases from 0.5 to 5.0 mol/L. This can be attributed to the charge attracting, which is an important mechanism for the phosphate adsorption in this material. Thus, coexistence of anion will compete with the adsorption sites, leading to the decrease in the adsorption capacity and in which the HCO_3^- possesses the highest affinity for the adsorption sites. In addition, a higher concentration of coexisting anions exhibited a much stronger competitive effect.

3.3. Adsorption mechanisms

From the above analysis, the highly affinity for SA-Ca-Ce bead toward phosphate may account for the existence of the electrostatic and Lewis acid–base interactions between the Ce^{3+} sites and the target

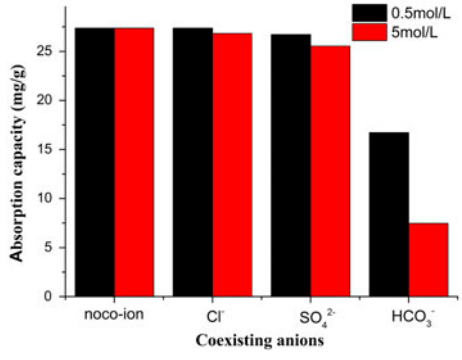

Fig. 8. Effect coexisting anions on phosphate adsorption, phosphate concentration of 100 mg/L, adsorbent dosage 2.0 g/L and temperature = 298 K.

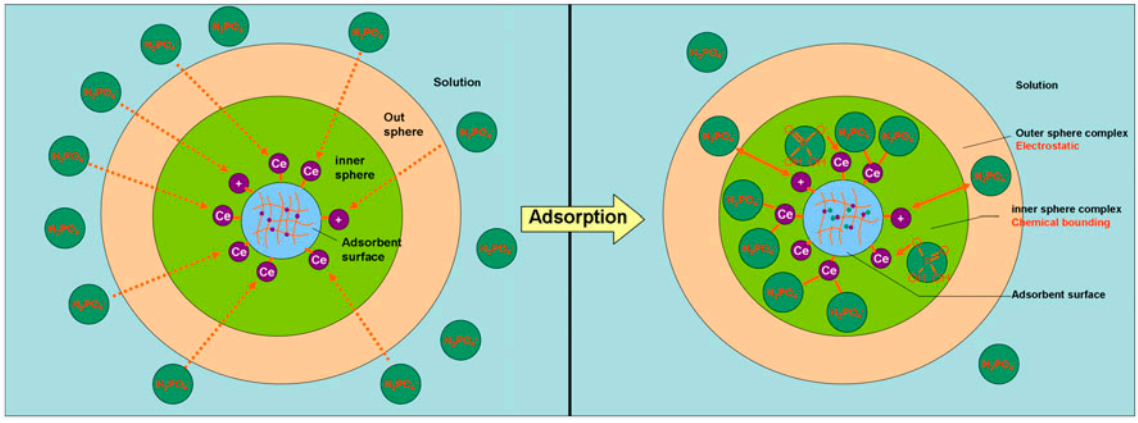

Fig. 9. Mechanism of phosphate uptake on SA-Ca-Ce bead.

anions in solution. The schematic description of the mechanism for phosphate adsorption on SA-Ca-Ce bead is illustrated in Fig. 9.

At the pH 2 (below the pH_{pzc}), SA-Ca-Ce bead represents positive-charged surface, leading to a strong electrostatic force toward anionic phosphate in the solution to form the outer sphere complex. Further, the oxygen anions of phosphate coordinate with the unoccupied orbital existed in the Ce^{3+} sites due to Lewis acid–base interaction.

With the increase of adsorption time, the phosphate is gradually diffused to the interior of the bead, more and more phosphates were adsorbed by the cerium active sites with chemical bonding. Meanwhile, coordinate bonds that for forming the cross-linked structure of SA were disconnected due to competitive effect of the oxygen anions of phosphate so that the partly cross-linked chain of the SA-Ca-Ce bead was broken which can be observed in the SEMs.

3.4. Stability

After adsorption of phosphate, the loss rate of Ce^{3+} and Ca^{2+} in the SA-Ce-Ca was 0.037 and 0.051%. It is an acceptable level of metal ion release, indicating that the adsorbent is stable in this process. The reason can be explained that most of the metal ions (Ce^{3+} and Ca^{2+}) are combined firmly in the interior of the bead, the phosphate would transfer into adsorption sites and form undissolved substance with metal ion *in situ* at the adsorption process, which is difficult to release into the water. Moreover, it is noted that the prepared SA-Ce-Ca has been washed with a large amount of deionized water for the complete removal of the adherent metal ion, which can also help reduce the loss of Ce^{3+} and Ca^{2+} after adsorption process.

4. Conclusion

In this study, a cross-linked cerium(III)-loaded alginate bead (SA-Ca-Ce) has been prepared successfully via a simple drop-sphere-forming method and acted as a highly efficient adsorbent for the phosphate removal. After adsorption, the P-adsorbed SA-Ca-Ce was conveniently separated from the aqueous solution due to the granular shape and could be used for plant fertilizer. The adsorption process followed pseudo-second-order kinetics and the adsorption rates were found to be controlled by the external diffusion at the initial stage followed by the intraparticle diffusion during the subsequent period. The adsorption equilibrium data could be better described by Langmuir isotherm model and the adsorption capacity of phosphate could achieve 41.39 mg/g under the optimal conditions. Thermodynamic constants supported spontaneous, endothermic, and entropy-driven nature of phosphate adsorption on SA-Ca-Ce. According to the study about competing effect of coexisting anions, the inhibition of coexisting anions in phosphate adsorption follows the order: $HCO_3^- > SO_4^{2-} > Cl^-$. Electrostatic interactions and Lewis acid–base interaction may play the main role in phosphate adsorption from the FT-IR and SEMs analysis.

Acknowledgements

This work was supported by the Public Service Project of the Chinese Ministry of Land and Resources (No. 201311024).

References

[1] G.T. Frumin, I.M. Gildeeva, Eutrophication of water bodies—A global environmental problem, Russ. J. Gen. Chem. 84 (2014) 2483–2488.

[2] D.J. Conley, H.W. Paerl, R.W. Howarth, D.F. Boesch, S.P. Seitzinger, K.E. Havens, C. Lancelot, G.E. Likens, Ecology: Controlling Eutrophication: Nitrogen and Phosphorus, Science 323 (2009) 1014–1015.

[3] V.H. Smith, D.W. Schindler, Eutrophication science: Where do we go from here? Trends Ecol. Evol. 24 (2009) 201–207.

[4] A. Gieseke, P. Arnz, R. Amann, A. Schramm, Simultaneous P and N removal in a sequencing batch biofilm reactor: Insights from reactor-and microscale investigations, Water Res. 36 (2002) 501–509.

[5] L.E. de-Bashan, Y. Bashan, Recent advances in removing phosphorus from wastewater and its future use as fertilizer (1997–2003), Water Res. 38 (2004) 4222-4246.

[6] L.M. Blaney, S. Cinar, A.K. Sengupta, Hybrid anion exchanger for trace phosphate removal from water and wastewater, Water Res. 41 (2007) 1603–1613.

[7] N. Kawasaki, F. Ogata, H. Tominaga, Selective adsorption behavior of phosphate onto aluminum hydroxide gel, J. Hazard. Mater. 181 (2010) 574–579.

[8] J.-H. Yuan, M.-H. Hu, Z.-H. Zhou, L. Wang, Kinetic and thermodynamic behavior of the batch adsorption of phosphate from aqueous solutions onto environmentally friendly barbecue bamboo charcoal, Desalin. Water Treat. 52 (2014) 7248–7257.

[9] X. Yuan, W. Xia, J. An, J. Yin, X. Zhou, W. Yang, Kinetic and thermodynamic studies on the phosphate adsorption removal by dolomite mineral, J. Chem. 2015 (2015) 1–8.

[10] M.R. Awual, A. Jyo, Assessing of phosphorus removal by polymeric anion exchangers, Desalination 281 (2011) 111–117.

[11] X. Cheng, X. Huang, X. Wang, B. Zhao, A. Chen, D. Sun, Phosphate adsorption from sewage sludge filtrate using zinc–aluminum layered double hydroxides, J. Hazard. Mater. 169 (2009) 958–964.

[12] S. Tanada, M. Kabayama, N. Kawasaki, T. Sakiyama, T. Nakamura, M. Araki, T. Tamura, Removal of phosphate by aluminum oxide hydroxide, J. Colloid Interface Sci. 257 (2003) 135–140.

[13] M.S. Onyango, D. Kuchar, M. Kubota, H. Matsuda, Adsorptive removal of phosphate ions from aqueous solution using synthetic zeolite, Ind. Eng. Chem. Res. 46 (2007) 894–900.

[14] E. Oguz, Removal of phosphate from aqueous solution with blast furnace slag, J. Hazard. Mater. 114 (2004) 131–137.

[15] W. Huang, S. Wang, Z. Zhu, L. Li, X. Yao, V. Rudolph, F. Haghseresht, Phosphate removal from wastewater using red mud, J. Hazard. Mater. 158 (2008) 35–42.

[16] P.R. Rout, P. Bhunia, R.R. Dash, A mechanistic approach to evaluate the effectiveness of red soil as a natural adsorbent for phosphate removal from wastewater, Desalin. Water Treat. 54 (2015) 358–373.

[17] E.W. Shin, J.S. Han, M. Jang, S.-H. Min, J.K. Park, R.M. Rowell, Phosphate adsorption on aluminum-impregnated mesoporous silicates: Surface structure and behavior of adsorbents, Environ. Sci. Technol. 38 (2004) 912–917.

[18] L. Zeng, X. Li, J. Liu, Adsorptive removal of phosphate from aqueous solutions using iron oxide tailings, Water Res. 38 (2004) 1318–1326.

[19] S.G. Lu, S.Q. Bai, H.D. Shan, Removal mechanism of phosphate from aqueous solution by fly ash, J. Hazard. Mater. 161 (2009) 95–101.

[20] J. Liu, Q. Zhou, J. Chen, L. Zhang, N. Chang, Phosphate adsorption on hydroxyl-iron-lanthanum doped activated carbon fiber, Chem. Eng. J. 215–216 (2013) 859–867.

[21] F. Xie, F. Wu, G. Liu, Y. Mu, C. Feng, H. Wang, J.P. Giesy, Removal of phosphate from eutrophic lakes through adsorption by in situ formation of magnesium hydroxide from diatomite, Environ. Sci. Technol. 48 (2014) 582–590.

[22] L. Zhang, L. Wan, N. Chang, J. Liu, C. Duan, Q. Zhou, X. Li, X. Wang, Removal of phosphate from water by activated carbon fiber loaded with lanthanum oxide, J. Hazard. Mater. 190 (2011) 848–855.

[23] H. Li, J. Ru, W. Yin, X. Liu, J. Wang, W. Zhang, Removal of phosphate from polluted water by lanthanum doped vesuvianite, J. Hazard. Mater. 168 (2009) 326–330.

[24] H. Deng, X. Yu, Adsorption of fluoride, arsenate and phosphate in aqueous solution by cerium impregnated fibrous protein, Chem. Eng. J. 184 (2012) 205–212.

[25] L. Zhang, Q. Zhou, J. Liu, N. Chang, L. Wan, J. Chen, Phosphate adsorption on lanthanum hydroxide-doped activated carbon fiber, Chem. Eng. J. 185–186 (2012) 160–167.

[26] L. Zhang, Y. Gao, M. Li, J. Liu, Expanded graphite loaded with lanthanum oxide used as a novel adsorbent for phosphate removal from water: Performance and mechanism study, Environ. Technol. 36 (2014) 1–10.

[27] S. Tian, P. Jiang, P. Ning, Y. Su, Enhanced adsorption removal of phosphate from water by mixed lanthanum/aluminum pillared montmorillonite, Chem. Eng. J. 151 (2009) 141–148.

[28] J. Bajpai, R. Shrivastava, A. Bajpai, Dynamic and equilibrium studies on adsorption of Cr(VI) ions onto binary bio-polymeric beads of cross linked alginate and gelatin, Colloids Surf., A 236 (2004) 81–90.

[29] A.K. Pandey, S.D. Pandey, V. Misra, Removal of toxic metals from leachates from hazardous solid wastes and reduction of toxicity to microtox by the use of calcium alginate beads containing humic acid, Ecotoxicol. Environ. Saf. 52 (2002) 92–96.

[30] J. Maheswaran, B. Meehan, N. Reddy, K. Peverill, S. Buckingham, Impact of rare earth elements on plant physiology and productivity, Rural Ind. Res. Dev. Corporation 1 (2001) 1–40.

[31] V. Rocher, J.-M. Siaugue, V. Cabuil, A. Bee, Removal of organic dyes by magnetic alginate beads, Water Res. 42 (2008) 1290–1298.

[32] D. Rassis, I. Saguy, A. Nussinovitch, Collapse, shrinkage and structural changes in dried alginate gels containing fillers, Food Hydrocolloids 16 (2002) 139–151.

[33] B. Dupuy, A. Arien, A.P. Minnot, FT-IR of membranes made with alginate/polylysine complexes. Variations with the mannuronic or guluronic content of the polysaccharides, Artif. Cells, Blood Substitues, Immobilization Biotechnol. 22 (1994) 71–82.

[34] C.C. Ribeiro, C.C. Barrias, M.A. Barbosa, Calcium phosphate-alginate microspheres as enzyme delivery matrices, Biomaterials 25 (2004) 4363–4373.
[35] S. Largergren, Zur theorie der sogenannten adsorption geloster stoffe [Adsorption theory of dissolved substances], Kungliga Svenska Vetenskapsakademiens, Handlingar 24 (1898) 1–39.
[36] G. Blanchard, M. Maunaye, G. Martin, Removal of heavy metals from waters by means of natural zeolites, Water Res. 18 (1984) 1501–1507.
[37] J. Zhang, Z. Shen, W. Shan, Z. Mei, W. Wang, Adsorption behavior of phosphate on lanthanum(III)-coordinated diamino-functionalized 3D hybrid mesoporous silicates material, J. Hazard. Mater. 186 (2011) 76–83.
[38] H. Zhu, R. Jiang, L. Xiao, G. Zeng, Preparation, characterization, adsorption kinetics and thermodynamics of novel magnetic chitosan enwrapping nanosized γ-Fe_2O_3 and multi-walled carbon nanotubes with enhanced adsorption properties for methyl orange, Bioresour. Technol. 101 (2010) 5063–5069.
[39] W. Weber, J. Morris, Kinetics of adsorption on carbon from solution, J. Sanit. Eng. Div. Am. Soc. Civ. Eng. 89 (1963) 31–60.
[40] S.G. Wang, X.W. Liu, W.X. Gong, W. Nie, B.Y. Gao, Q.Y. Yue, Adsorption of fulvic acids from aqueous solutions by carbon nanotubes, J. Chem. Technol. Biotechnol. 82 (2007) 698–704.
[41] R. Han, W. Zou, W. Yu, S. Cheng, Y. Wang, J. Shi, Biosorption of methylene blue from aqueous solution by fallen phoenix tree's leaves, J. Hazard. Mater. 141 (2007) 156–162.
[42] D. Duranoğlu, İ.G. Buyruklardan Kaya, U. Beker, B.F. Şenkal, Synthesis and adsorption properties of polymeric and polymer-based hybrid adsorbent for hexavalent chromium removal, Chem. Eng. J. 181–182 (2012) 103–112.